Kinetochore Microtubules in PTK Cells

Kent L. McDonald, Eileen T. O'Toole, David N. Mastronarde, and J. Richard McIntosh

Laboratory for Three-dimensional Fine Structure, Department of Molecular, Cellular, and Developmental Biology, University of Colorado, Boulder, Colorado 80309-0347

Abstract. We have analyzed the fine structure of 10 chromosomal fibers from mitotic spindles of PtK_1 cells in metaphase and anaphase, using electron microscopy of serial thin sections and computer image processing to follow the trajectories of the component microtubules (MTs) in three dimensions. Most of the kinetochore MTs ran from their kinetochore to the vicinity of the pole, retaining a clustered arrangement over their entire length. This MT bundle was invaded by large numbers of other MTs that were not associated with kinetochores. The invading MTs frequently came close to the kinetochore MTs, but a two-dimensional analysis of neighbor density failed to identify any characteristic spacing between the two MT classes. Unlike the results from neighbor density analyses of interzone MTs, the distributions of spacings between kinetochore MTs and other spindle MTs revealed no evidence for strong MT–MT interactions. A three-dimensional analysis of distances of closest approach between kinetochore MTs and other spindle MTs has, however, shown that the most common distances of closest approach were 30–50 nm, suggesting a weak interaction between kinetochore MTs and their neighbors. The data support the ideas that kinetochore MTs form a mechanical connection between the kinetochore and the pericentriolar material that defines the pole, but that the mechanical interactions between kinetochore MTs and other spindle MTs are weak.

CHROMOSOME movements during mitosis appear to result from motor enzymes coupled to the controlled assembly and disassembly of spindle microtubules (MTs)[1] (reviewed in Rieder, 1990; McIntosh and Hering, 1991; Sawin and Scholey, 1991). Building on this overview to develop a full understanding of chromosome motion will require not only an identification of the relevant motor enzymes and a description of their roles and locations, but also a characterization of the mechanical linkages that connect chromosomes to the rest of the mitotic machinery. Spindle MTs are an essential part of this linkage system; they connect kinetochores with spindle poles (for example see Nicklas and Kubai, 1985), poles with poles (Leslie and Pickett-Heaps, 1983), and poles with some as yet poorly defined aspect of the cell cortex (Aist and Berns, 1981; Hamaguchi and Hiramoto, 1986; Hyman, 1989). Just how these connections are made is still largely unknown, because an understanding of linkage depends both upon locating the ends of the relevant MTs and identifying the connections that each MT makes with other MTs or with other structural material in the cell. Such knowledge requires information available only by EM, because most spindle MTs are bunched so closely together that they cannot be resolved from one another in the light microscope; an apparently continuous fiber can be composed of either a few long MTs or a cluster of short ones. For example, the MT bundles that run from pole to pole have long been called "continuous fibers" (Schrader, 1953), but EM has shown them to be composed of two sets of MTs that emanate from the poles and interdigitate near the spindle equator (Paweletz, 1967; McIntosh and Landis, 1971; McDonald et al., 1977). This distinction is important because recent evidence demonstrates that spindle elongation occurs by MT polymerization at the zone of interdigitation, together with MT sliding driven either from the zone of interdigitation or from the asters (Aist and Bayles, 1991; Saxton and McIntosh, 1987; Masuda et al., 1988; Hogan and Cande, 1990). Such a mechanism would be impossible with truly continuous MTs.

The spindle fibers that connect chromosomes with poles display even more complex behavior. They are essential parts of the machinery for both chromosome congression to the spindle equator during prometaphase and poleward motion during anaphase A (reviewed in Rieder, 1982; Mitchison, 1988; McIntosh and Hering, 1991). Studies on the forces generated by a normal spindle demonstrate that a chromosomal fiber can pull on its chromosomal connection more strongly than is necessary to overcome viscous drag (reviewed in Nicklas, 1988). Experiments in vitro (Mitchison and Kirschner, 1985; Hyman and Mitchison, 1991) and descriptions of chromosome behavior in vivo (for example see Tippit et al., 1980) suggest that a chromosomal fiber can also push a kinetochore away from the pole it faces. The fiber elongates or shortens largely by the addition or loss of tubulin at its kinetochore-proximal end (Mitchison et al., 1986;

1. *Abbreviations used in this paper*: kMT, kinetochore microtubule; MT, microtubule.

Gorbsky et al., 1988; Nicklas, 1988), but during metaphase, when each fiber is on average of constant length, it can add tubulin at the kinetochore and lose it at the pole, resulting in a poleward flux of tubulin subunits (Mitchison, 1989). Chromosomal fibers are clearly important in their action, and the complexity of their behavior suggests that understanding them will require detailed study.

EM of chromosomal fibers has revealed that they always include one or more MTs associated with each kinetochore. Usually these MTs end at the kinetochore, whereupon they are called kinetochore MTs (kMTs). Other features of chromosomal fibers, however, display a discouraging diversity of design that confounds simple interpretation. The chromosomes of lower eukaryotes appear to be linked to the spindle pole by one or a few kMTs that run all the way from kinetochore to pole (reviewed in Heath, 1980; McDonald, 1989; McIntosh and Hering, 1991). Chromosomal fibers of higher eukaryotes, however, are usually composed of many MTs and comprise more than one MT type (reviewed in Rieder, 1982, 1990; McDonald, 1989). In the green alga *Oedogonium* there are ~40 kMTs in each chromosomal fiber, but most of these extend only about one quarter of the way to the pole; none is long enough to reach the pole, so the 15-μm chromosomal fiber characteristic of the metaphase spindle is composed largely of non-kMTs (Schibler and Pickett-Heaps, 1987). In the higher plant *Haemanthus* most kMTs again appear to be short relative to the distance from chromosome to pole, and during anaphase they both decrease in number and fan out as the chromosome approaches the pole (Jensen, 1982). Chromosomal fibers in meiotic spindles of crane flies appear to be organized differently, though there is some disagreement about details. One group has reported that they are formed from clusters of many short MTs that link the chromosome to the pole indirectly (for example, see Fuge, 1985), while another group has found longer kMTs, some of which reach all the way from kinetochore to pole (Scarcello et al., 1986). This distinction is important because the former implies the existence of MT–MT interactions that are strong enough to support the mechanical load of positioning and moving a chromosome, while the latter implies a direct MT linkage between each kinetochore and the pole it faces.

The discrepancies cataloged here suggest that there is variability in the design of chromosomal fibers, so reliable structure–function correlations demand that fine structure work be done on the cells for which physiological and biochemical data are available. We have therefore undertaken a study of chromosomal fibers in the mammalian cell line, PtK, which is routinely used for light microscopic studies of mitotic physiology (for example, see Mitchison, 1989). Detailed structural work on mammalian spindles is daunting, because they contain so many MTs and because large numbers of sections are required for a three dimensional (3-D) picture of the spindle. In the studies on chromosomal fibers of mammalian cells published thus far, the problem has been simplified by using an experimental perturbation to reduce the number of spindle MTs. With this strategy it has been shown that the chromosomal fibers of cold-treated PtK_1 cells include some MTs that run all the way from kinetochore to pole, many that have one end on a kinetochore and the other free in the fiber, many that have one end at the pole with the other free in the fiber, and some with both ends free within the fiber (Rieder, 1981). In CHO cells recovering from colcemid treatment, the chromosomal fiber is comparatively short, and over 90% of the kMTs run most of or all the way from chromosome to pole (Witt et al., 1981). In both of these studies, however, many of the non-kMTs were removed from the spindles by experimental treatment, so the contribution that these polymers might make to the structure of the normal chromosomal fiber could not be assessed.

Recent advances in the methods and hardware for computer image processing have made it possible to reduce the labor required to process data from the serial cross sections required for a 3-D reconstruction of spindle structure (McDonald et al., 1991). Here we capitalize on this technology to study the chromosomal fibers of PtK cells and to characterize both their kMTs and non-kMTs at different times between metaphase and late anaphase. Our analysis suggests that spindle design in PtK cells is much like that of the lower eukaryotes; some kMTs connect each kinetochore directly with the pole it faces. The kMTs do not appear to interact strongly with the non-kMTs, but a close, quantitative scrutiny reveals subtle evidence for a linkage between the two. Our work supports the idea that a bundle of kMTs forms a mechanical connection between each kinetochore and the material that surrounds the centrosome. This MT bundle probably transmits tension from wherever the mitotic motors may generate it to the mechanical linkages required for moving the chromosomes to the equator during prometaphase and pulling them poleward in anaphase.

Materials and Methods

Electron Microscopy

PtK_1 cells were grown on glass coverslips and fixed for EM as described by McDonald (1984). Cells were flat-embedded by inverting the coverslip/cells onto a drop of Epon-Araldite on a slide coated with MS-122 PTFE release agent (Miller Stephenson, Los Angeles). After resin polymerization was complete, the coverslip was dissolved with hydrofluoric acid (Moore, 1975), and the wafer of resin with cells was taped to a microscope slide. The wafers were scanned with phase optics at 40×, and appropriate mitotic stages were scored and remounted for serial cross sectioning. Serial 75-nm sections were picked up on 1 × 2 mm formvar-coated slot grids and poststained with lead and uranium. Sections through kinetochore fibers were photographed at a magnification of 16,000 or 21,000 on a Philips CM10 electron microscope (Philips Electronic Instruments Co., Mahwah, NJ) operating at 80 kV.

Data Entry and Three-dimensional Reconstruction

The details of how images of spindle cross sections were entered into computer memory and aligned, how the MTs in successive sections were identified and connected to build models, and how these models were edited to form accurate representations of spindle MT geometry are described in McDonald et al. (1991). Briefly, a Dage 81 video camera (Dage-MTI, Inc., Michigan City, IN) was used to image EM negatives of successive sections, and this signal was digitized by a Parallax 1280 graphics device in a MicroVax III computer (Digital Equipment Corp., Maynard, MA). We used 10–12 pixels/MT diameter, so our 640 × 480 pixel frames included ~1.25 μm^2 of spindle cross section, enough to include a kinetochore and about eight times that area surrounding the kinetochore in each data set. We selected kinetochores that lay near the spindle axis to minimize the curvature of the associated chromosomal fiber, found the section that contained the kinetochore, backed up 5–10 sections into the chromosome proper, and then digitized corresponding areas of each successive section all the way to the first centriole.

The images were aligned upon entry into the computer by comparing the most recently stored image with the live image from the camera and adjusting the position of the negative to make the two as similar as possible. Accurate MT tracking required better alignment than could be achieved by

translations and rotations alone, because the images of some sections were distorted by sectioning compression or beam-induced shrinkage. The alignment of the digitized images was therefore refined by marking the positions of 6–8 MTs in good transverse view to identify corresponding points on successive sections. These points were used to define a general linear transformation (translation, rotation, magnification, and uniaxial stretch) to optimize the fit of each image with its neighbors. The transformation for each section was then combined with transforms for the six nearest sections in a way that removed section–section misalignments, yet preserved long-term trends in the transformations, such as the convergence of MTs toward the spindle poles.

Aligned images were then cross-correlated with an image of an average MT and a linear discriminant analysis was applied to all regions of high correlation to identify those points that most resembled true MTs (for details see McDonald et al., 1991). The resulting trial set of MT locations was used by the computer to track MT positions from section to section; points on adjacent sections were connected when they lay within 15 pixels (~1.3 MT diams). These computer-generated models were then displayed as graphic overlays on the image data, and a trained biologist examined the MT identifications and connections for errors. In general, the computer-generated models included a few false points and were missing ~15% of the MTs, but these errors could be corrected rather quickly with the interactive display. When the display was made to move rapidly from one section to its well-aligned neighbors, successive images of each MT were readily recognized, even when the MT was highly oblique to the plane of section. Thus, the accuracy of the model at any stage of completion was easy to assess. Early in our work we reconstructed the same data set several times in several ways, each time with different people involved. Whenever the method included a final editing in which an operator riffled rapidly through multiple sections, comparing the images of each MT with the model points presented as a colored overlay, the resulting models were essentially the same. We are therefore confident that our completed models are reliable. Further, the identification of kMTs was always checked by at least two people. Note, however, that the final models do not include every MT that entered the volume defined by the digitized images. We made sure that every MT that approached or joined the kMT bundle was included, but the few non-kMTs that skirted the periphery of the volume under study and never came close to the kMTs were omitted for clarity.

Before analyzing a completed model, we generated a new alignment of the serial sections, using general linear transformations derived from all of the MT positions in the completed model. This alignment generally produced an excellent fit between adjacent sections, so the MT positions progressed smoothly from section to section. We were thus able to represent MTs simply as a set of line segments connecting the modeled points with no need for further smoothing of the MT trajectories.

Neighbor Density Analysis

To analyze the distributions of MT positions in spindle cross sections, we represented the center of each MT by a point in a plane, calculated the number of points per unit area as a function of distance from each individual point, and then averaged the resulting density distributions over all points (Boots and Getis, 1988; Rodieck, 1991). The densities were computed in "bins," each representing a range of distance from the central point under consideration. To obtain the density for a particular bin, e.g., from 36 to 48 nm from the central point, one would place the appropriate annulus around each point analyzed; Fig. 1 *A* shows three such annuli drawn on a set of points that represent a bundle of interdigitating MTs from a PtK_1 cell in telophase. Ideally, one could then add up the number of points falling in each of the annuli of a given radius and the area covered by each of the annuli; neighbor density at that radius would then be the total number of points divided by the total area of those annuli.

This simple approach is, however, inaccurate when the points being analyzed occupy a finite region. One way to deal with this problem is to specify a boundary around the points and to omit from the area summation those portions of the annuli that fall outside the boundary. We have written a program to deal with regions of arbitrary shape by explicitly calculating the fraction of each annulus that lies within the boundary. This method requires one to choose a specific boundary by drawing a series of line segments around the points under consideration. We placed our boundaries so as to follow the major irregularities in the region and to maintain a distance from the outermost points that was between one half and one times the typical distance between adjacent MTs (see boundaries drawn in Fig. 1 *A*). This practice generally resulted in density graphs that were flat at large distances (e.g., Fig. 1 *B*, which shows neither an upward or downward trend from 100–300 nm). The density graphs were fairly insensitive to the specific choice of boundary within these guidelines, but with a much looser boundary, such as a convex polygon surrounding the points, the graph showed a downward trend, and a tighter boundary produced a slight upward trend at large distances.

When these methods are used to analyze the neighbor density distribution of a random array of points, a flat density graph is obtained (data not shown). This feature of the analysis has provided us with a simple way to measure the strength of the deviation from randomness for any particular data set. First, we obtained a mean density value from the flat portion of the graph at large radial distances, then we determined the range of distances over which the graph deviated from randomness (e.g., the peak between 36 and 48 nm for telophase MTs shown in Fig. 1 *B*). The deviations from mean density were then multiplied by the appropriate annular areas and summed over that range of distances; the resulting integral indicates the number of MTs, above those expected in a random distribution, that were positioned at this range of distances from the typical MT. For Fig. 1 *B*, the integral is 2.75 extra MTs surrounding the typical MT at distances between 36 and 48 nm.

When more than one type of point is present, it is possible to measure the density of a particular kind of point as a function of distance from some other kind(s) of point by summing over annuli placed around a subset of points and counting only the neighbors of a particular type. Thus, Fig. 1, *C* and *D* show the density of telophase MTs from the same pole, or from the opposite pole, as a function of distance from each MT, averaged over

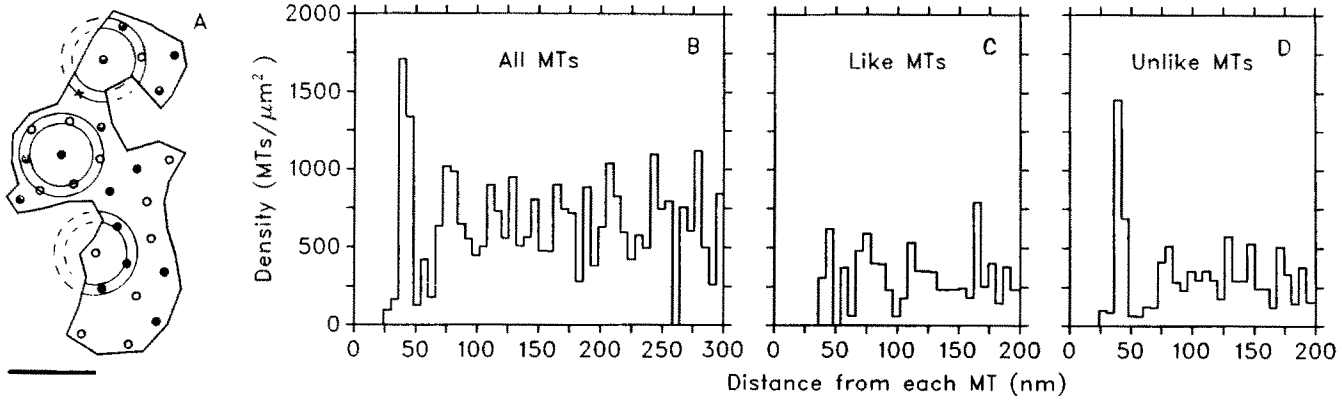

Figure 1. Neighbor density analysis of a microtubule (*MT*) bundle from the interzone of a PtK_1 spindle in telophase. (*A*) A model of MT positions from a transverse section and a boundary traced around the bundle. The annuli shown are three of the many involved in computing neighbor density between 36 and 48 nm. Filled and open circles mark MTs that were identified as coming from one spindle pole or the other; the cross marks the one MT whose polarity was ambiguous. (*B*) The density of MTs of any type, as function of distance from each MT in *A*. (*C* and *D*) The density of MTs from the same pole, or from the opposite pole, as a function of distance from each MT. Bar, 100 nm.

all MTs in the interzone MT array shown as Fig. 1 *A*. The occurrence of MTs at a preferred distance shows a high degree of specificity by type; integrals from 36 to 48 nm indicate that the typical MT has 2.34 extra neighbors from the opposite pole but only 0.51 extra neighbors from the same pole. We interpreted this sort of preference as a measure of positional specificity and infer that the departure from randomness is due to a specific interaction between two kinds of MTs (for example, see McDonald et al., 1979).

When a density graph shows evidence for a specific interaction, it is important to assess the probability that such a graph could have been obtained by chance from a distribution of points that does not include such an interaction. Often, an appropriate test is to construct a random sample of points, subject to the constraint that they be separated by a minimum distance. A more appropriate test for the specificity seen in Fig. 1, *C* and *D* is to randomly shuffle the identities of the MTs. After the types in this data set were shuffled 50 times, the integral for MTs from the same pole had a mean ± SD of 1.28 ± 0.38 and was less than the actual value of 0.51 only once. The integral for MTs from the opposite pole was 1.36 ± 0.38 and never exceeded the actual value of 2.34. Such a method provides a measure of the statistical significance of the difference between the density graphs in Fig. 1, *C* and *D*.

Three-dimensional Analysis of Closest Approach between Microtubules

Many of the MTs in a chromosomal fiber approach each other at a wide variety of angles (see Figs. 4 and 5). We therefore analyzed the distances of closest approach between these MTs in 3-D. To do so, MTs were treated as a series of line segments connecting the centers of MT images on successive serial sections. Each MT (or each MT of a particular type) was taken in turn as a "reference" MT. The closest approach between the reference MT and each other MT (or each other MT of a particular type) was identified. The distances of closest approach were then counted in bins, with each bin representing a range of distances. These counts were divided by the number of reference MTs, and the resulting value for a particular bin was the average number of MTs having a closest approach at that range of distances from the reference MTs.

Several problems inherent in this type of spatial analysis have not been as completely solved for the 3-D analysis as for the 2-D case. For example, there is no obvious way to correct for boundary effects. Data are presented here without any boundary effect corrections for two reasons. First, such effects should not contribute very much to the distribution of distances of closest approach between kMTs and non-kMTs, because all of the non-kMTs approaching within about 500 nm of the kinetochore bundle were included in the reconstruction. Second, even when there are boundary effects that cause the distribution of neighbors to decline at large distances, such declines are gradual and, as will be seen, they do not obscure the rather sharp peaks that reflect the short-range interactions of interest.

Another problem with the 3-D analysis is in scaling the counts of neighbors so they will represent a density. Our main goal was to scale the data so that randomly distributed MTs would show a flat graph, thus facilitating the detection and measurement of deviations from randomness. If we had been analyzing the positions of points in either two or three dimensions, then a graph proportional to density could have been obtained by dividing the number of points at a given distance from a point by either distance (in the 2-D case) or distance squared (in the 3-D case). We therefore experimented with dividing by a power of distance. Generalizing from the scaling of 2- and 3-D point distributions, we divided each bin by (Bin width) $\times \pi(2 \times \text{Distance})^p$, where p is the power to which the distance is to be raised. We refer to the resulting scaled values as relative densities. With $p = 0.4$, graphs were nearly flat between ~75 and 200–300 nm, beyond which the relative density generally declined because of boundary effects.

Because the value of 0.4 seemed arbitrary, we also analyzed some distributions of closest distances after shifting the position of each MT by a random amount parallel to the plane of section. When the log of unscaled counts was plotted versus the log of minimum distance, the points fit a straight line fairly well over most of the range of distance; the slopes of these graphs were near 0.4. This indicates that scaling by distance to the 0.4 power is a good approximation for obtaining relative densities.

The distributions of distances of closest approach presented in this paper were all graphed with a scaling of 0.4 because in this way the departures from randomness were easier to see. The scaling also allowed a good estimation of the strength of any peak in the distribution. The average relative density from 100 to 200 nm was subtracted from the density in each bin representing the peak region. The result was then unscaled and summed over the bins to obtain the number of MTs, above those expected by chance, approaching to within that range of distances from the typical reference MT. Note that our choice of scaling does not affect our conclusions, because all subsequent analysis was based on a comparison of the integrals and the relative densities for actual data with the corresponding integrals and relative densities for randomized data.

A final difficulty with the 3-D analysis has been the construction of meaningful random data sets for comparison with actual data. Curves following random trajectories in 3-D space have too few of the features of chromosomal fibers to be useful for comparison. The real data were therefore "randomized" by shifting each MT (or each MT of a particular kind) by a random amount in x- and y-axes (i.e., within the plane of section). We were usually interested in assessing whether a preferred distance of closest approach could be attributed simply to the inability of two MTs to approach closer than that distance. Thus, for each MT being shifted, a potential shift was evaluated by checking the minimum distance of closest approach to all of the other MTs that had already been placed in their final positions. If that minimum distance was less than a certain amount, chosen to reflect the actual distributions, then the potential shift was subject to rejection, where the probability of rejection was a function of distance, as chosen by the operator to reflect the actual distributions. The program would try up to 300 shifts with the original range of shifts, up to 150 shifts with 1.5 times that range, and up to 150 shifts with 2.0 times that range. If all trials were rejected, the MT was left unshifted. Most MTs could be shifted in only 1–3 trials, but some required many trials and a few could not be shifted. To provide the most realistic test, the probabilities of rejection were adjusted so that the rising phase of the resulting graph of relative density of closest approach versus distance matched that of the unshifted data. Probabilities were specified for ranges of distance equal to the bin size in the density graph and were thus uniquely determined by the graph being matched. The probabilities used were 1.0 from 0 to 15 nm, then fell gradually to 0 by 35 nm.

Results

Images of PtK Spindle Microtubules

The longitudinal section through a PtK metaphase half spindle, shown in Fig. 2, illustrates a number of points relevant to this study: (*a*) the fixation of our material is good, as revealed by the smooth contours of vesicles and the generally straight appearance of MTs. Where the MTs are curved, e.g., those running from the chromosomes at an edge of the metaphase plate, the curves follow smooth arcs, not the wavy paths characteristic of poor fixation. (*b*) For this investigation we have usually analyzed chromosomal fibers from the central region of the spindle to take advantage of the straight trajectories of their MTs. (*c*) Kinetochores are not always flat structures (e.g., Ks 4 and 5). Thus, in cross sections like those shown in Fig. 3, one would not expect to find all the kMTs ending in a single section, even when the plane of section is exactly perpendicular to the chromosomal fiber. (*d*) the spindle pole is a region that extends some distance from the surface of the centrioles. In these cells it is marked by electron-dense pericentriolar material. It is not possible to identify the outer boundary of the pericentriolar material with precision, but it is recognizable 0.2–0.5 μm from the surface of the parent centriole. We have regarded this entire region as the spindle pole. (*e*) In the longitudinal section, the spindle appears to be composed of many relatively short, overlapping MTs. These short pieces are actually segments of longer MTs that course through several sections. We have found it difficult or even impossible to track individual MTs from one longitudinal section to the next, particularly where the MTs are bunched together near the poles. We therefore have chosen to use serial cross sections for making 3-D reconstructions.

Fig. 3 is a series of cross sections through the kinetochore

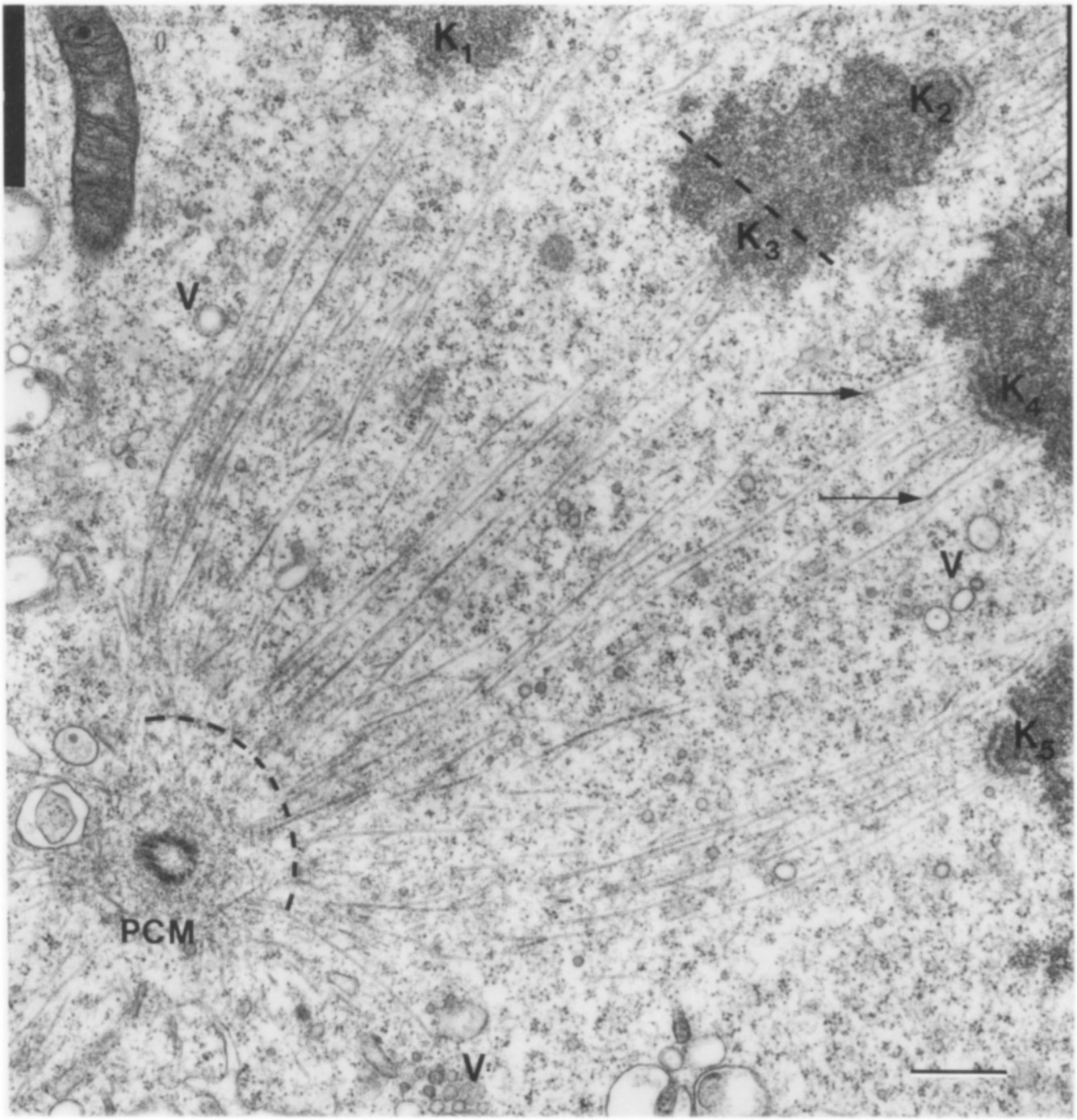

Figure 2. Conventional EM view of a PtK_1 spindle in metaphase, showing a pole, as defined by the oblique section of a centriole and the pericentriolar material (*PCM*), spindle MTs, and parts of five different kinetochores labeled K_{1-5}. Good quality fixation is indicated by the smooth contour of vesicles (*v*) and the straightness of the MTs (e.g., the group running between K_3 and the pole). KMTs that leave the plane of section (*arrows* on MTs associated with K_4) appear artificially short in longitudinal sections. The pericentriolar material around the centriole is an indicator of the spindle pole boundary; in serial cross sections, this boundary usually appeared ~0.4–0.5 μm from the centrioles (*curved dotted line*). The straight dotted line behind K_3 indicates where we have begun MT tracking (see Fig. 3 *A*). Bar, 0.5 μm.

region of a metaphase chromosome. Throughout this study we have identified kMTs by starting a reconstruction well within the chromosome itself (see the marking line in Fig. 2 and the image shown in Fig. 3 *A*). As one moves through the serial sections toward the pole, the kinetochore is readily identified by its characteristic staining, which is delimited by a dashed line in Fig. 3 *B*. In Fig. 3, *C* and *D* one finds a number of closely packed MTs beginning within a few sections. These we have designated kMTs. The additional MTs that join the kMT cluster between the kinetochore and the pole

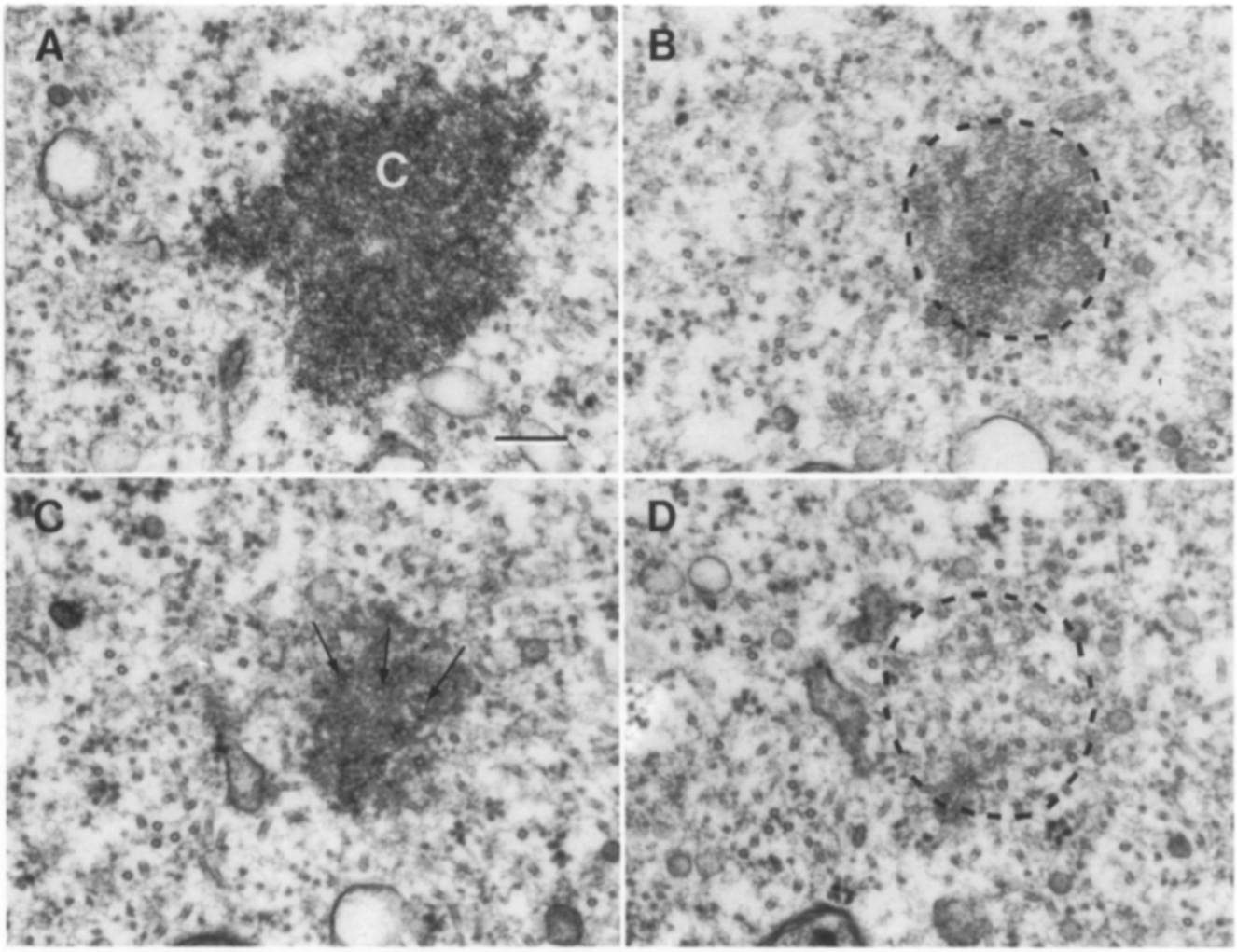

Figure 3. Images of sections near a kinetochore that illustrate how we decided which were kMTs. In *A*, we marked MTs around the chromosome (white *C*), well behind the kinetochore, so we would know that all these were non-kMTs (see Fig. 2). (*B*) A cross section through the light-staining middle region of the trilaminar kinetochore. The dotted line indicates the boundary of the kinetochore. Note that no new MT cross sections can be seen within this region. (*C*) The serial section adjacent to *B*; it passes through the outer dark plate of the kinetochore. Some MT profiles are now evident (*arrows*). The next adjacent serial section (*D*) includes the profiles of most of the kMTs for this fiber within an area equal to that of the kinetochore (*dotted line*). However, not all MTs within the dotted line area are kMTs. Note that the area of each of these panels approximates the areas digitized for 3-D reconstruction. Bar, 0.2 μm.

are called non-kMTs. While it is possible, a priori, that some of these might be kMTs from a different chromosomal fiber, this is highly unlikely. The kMTs as seen in serial cross sections form a definite bundle that changes relatively little as one approaches the pole (see Fig. 4 *C*). If all kMTs follow well defined bundles, then the MTs that wander into a bundle and are not themselves bundled cannot be kMTs. Indeed, a reconstruction of five kinetochore fibers that associate with the same pole has shown that the bundles of kMTs remain distinct throughout their lengths (data not shown). In the immediate vicinity of the poles, some of the MTs that join the edge of a chromosomal fiber might be kMTs from other chromosomal fibers, but these represent only a small fraction of the MTs under study.

Models of Chromosomal Fibers during Metaphase and Anaphase

The geometrical accuracy of our models is dependent upon the ability of embedding, sectioning, and EM to preserve 3-D relationships from the living cell. Our need to use a general linear transformation to align images of successive sections demonstrates that at least some of our images were distorted. Without an external standard for comparison, we were not able to transform each image to a distortion-free geometry, but our methods did allow us to remove any major distortion and make the residual distortions uniform. This statement is supported by the smoothness of the curves that represent MTs in the models; these look much like the MTs in Fig. 2. We estimate that the residual distortions are <5%. To measure lengths in the dimension perpendicular to the plane of section we used the average section thickness, as defined by both the setting on the microtome and the interference color of the sections as they floated beside the knife edge. This procedure was checked by counting the number of sections necessary to get from one spindle pole to the other and comparing this with light micrographs taken of the same fixed, embedded cell before its excision and mi-

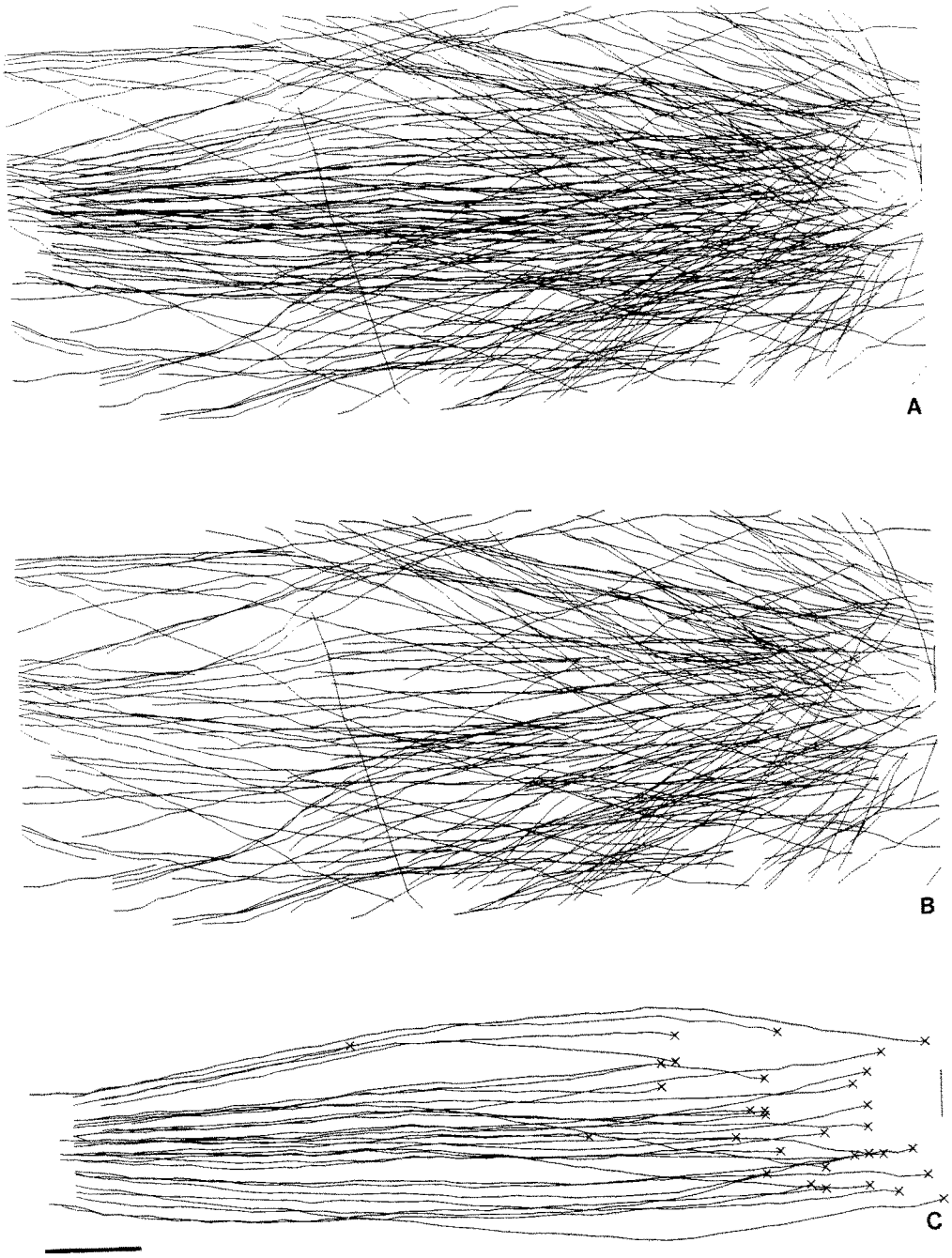

Figure 4. Reconstructions of a metaphase chromosomal fiber, displaying both kMTs and non-kMTs. The bundles are oriented with the kinetochores on the left and the polar regions at the right. The vertical bars in each drawing mark the section containing the first image of a centriole. (*A*) All the MTs in the fiber bundle; (*B*) only the non-kMTs. Many of these run oblique to the fiber axis, and near the pole they are more numerous. (*C*) Only the kMTs. (*X*) The pole-proximal end of each kMT. Bar, 0.5 μm.

crotomy. The nominal section thickness of 75 nm agreed with the calculated thickness to within 5%, so the dimensional accuracy of our models is approximately isotropic.

We have used computer technology to trace the trajectory of each spindle MT in 10 chromosomal fibers and to map them in 3-D. An overall impression of the resulting structures can be obtained by viewing all the MTs of the bundle simultaneously. Such complex and disordered structures are most easily understood when displayed in color on a monitor capable of dynamic, 3-D display. Since these displays cannot be published, and since even stereo projections in color are of limited value (see Fig. 5 in McDonald et al., 1991), we have opted here to show the different classes of MTs as separate black and white projections. Fig. 4 *A* shows all the MTs of one metaphase chromosome fiber; Fig. 4, *B* and *C* show the non-kMTs and kMTs, respectively, from the same fiber. Compared with the more conventional view of spindle structure provided by Fig. 2, one is struck by the large number of non-kMTs that are associated with the kMTs, running both parallel and skew to the axis of the bundle. Indeed, Fig. 4 *A* raises a question of why chromosomal fiber appears in the light microscope as such discrete objects, using either polarization, differential interference contrast (DIC), or fluorescence optics. 3-D EM, which detects and displays all the MTs that have been fixed, suggests that the chromosomal fiber is both more complex and less independent than has been suggested by light microscopy.

The chromosomal fibers we have studied contain a rather

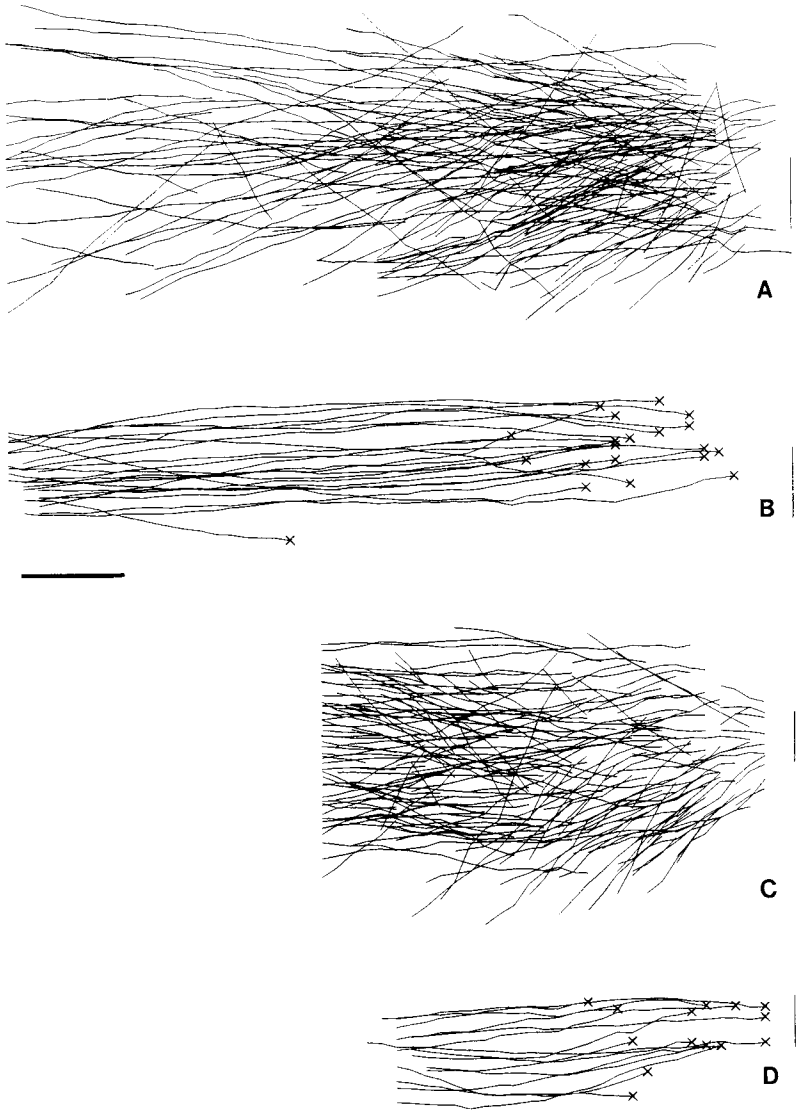

Figure 5. Reconstructions of chromosomal fibers from mid and late anaphase PtK_1 cells. (*A*) Non-kMTs; (*B*) kMTs from a mid anaphase fiber. As in metaphase, there is a greater density of non-kMTs near the pole. The vertical bars again mark the positions of the first appearance of a centriole. (*C*) Non-kMTs; (*D*) kMTs from a late anaphase spindle. At this stage, non-kMTs are prevalent along the entire length of the kinetochore bundle. Bar, 0.5 μm.

uniform number of kMTs, and these stay relatively close together all the way from the kinetochore to the pole (Fig. 4 *C*). Four metaphase fibers contained 25.5 ± 5.2 kMTs, three mid-anaphase fibers had 25.0 ± 2.1 kMTs, and three late anaphase fibers had 20.3 ± 3.1. The total MT densities in a typical metaphase fiber cross section were 141 MT/μm^2 at the kinetochore, 121 MT/μm^2 midway to the pole and 140 MT/μm^2 at the pole. These total densities included kMTs, which are at high density near the kinetochore but disperse slightly as they run poleward, and non-kMTs, which disperse at the kinetochore and focus in as they approach the pole (Figs. 4 and 5). The overall design of the fiber changes little with time from metaphase to anaphase.

This study included no effort to find the pole-distal ends of all the non-kMTs. We have defined the volumes for reconstruction so as to be sure to include all the kMTs of a given chromosomal fiber but have not tried to follow the more oblique non-kMTs as they diverged from the fiber axis. Between 2 and 10 non-kMTs per chromosomal fiber stayed close enough to the kMTs to follow to their true ends, but most of the non-kMT pole-distal ends in our models are artifactual, created by the boundaries of data collection.

Distributions of Kinetochore Microtubule Lengths

Our 3-D reconstructions of chromosomal fibers allow a complete description of the distribution of kMT lengths. Most of the kMTs are long enough during both metaphase and anaphase to have their kinetochore-distal ends in the vicinity of the pole (Figs. 4 and 5). Most of the 238 kMTs we have tracked ended within 1 μm from the nearest centriole (Fig. 4 *C*; x, the pole-proximal ends of the kMTs). Our electron micrographs do not allow us to say whether these ends are "at the pole," because the amorphous, pericentriolar material is too ill-defined to permit a confident description of its distribution. Our interpretation of the data is that most of the kMTs are associated with polar material, but some have detached, reflecting, perhaps, the tendency for a centrosome to cast off the MTs it initiates (Vorobjev and Nadenzhdina, 1987).

Fig. 6 shows Tukey box plots (Cleveland, 1985) of the distributions of kMT lengths from the fibers we have reconstructed (see legend for details). Both the median and the spread of the kMT lengths decrease as the chromosomes approach the poles, as one would expect for anaphase A, but

the spread in the range of the longest 75% of the kMTs (the distance from the bottom of each rectangle in the Tukey boxes to the top of that distribution) changes very little with time (0.95 μm in metaphase, 0.84 μm in mid-anaphase, and 0.99 μm in late anaphase). These data, together with the similar appearance of the kMT minus end distributions in Figs. 4 and 5, suggest that the pole-proximal ends of the kMTs are not significantly restructured during anaphase.

The chromosomal fibers studied included some "free MTs," i.e., polymers whose ends are both free from attachment to identifiable spindle structures. The metaphase, mid-anaphase, and late anaphase fibers contained averages of three, three, and two free MTs, respectively. These numbers are low enough to suggest that such fragments play no important role in the mitotic mechanisms of PtK cells.

Microtubule Trajectories Visualized in Selected Cross Sections

From the 3-D models of chromosomal fibers it is difficult to determine whether kMTs and non-kMTs lie at particular spacings from one another in such a way as to suggest specific interaction. Certainly the two classes of MTs intermingle, but in the longitudinal projections there is no obvious pattern to the MT associations. One can get a better sense of the MT mixing that occurs by taking a portion of the fiber, e.g., nine successive sections, and displaying it in transverse orientation (Fig. 7). From such a display it is evident that the non-kMTs have a greater tendency to move across and through the MT cluster than do the kMTs.

Another way to visualize this intermingling of the two MT types is to take cross sections from near the kinetochore, near the pole, and from a region in between, then use different symbols to represent each MT type (Fig. 8, *A–C*). At the kinetochore of a metaphase chromosomal fiber (Fig. 8 *A*), the kMTs are tightly bunched, and the non-kMTs form a more or less distinct bundle. By halfway to the pole (Fig. 8 *B*) there is already considerable infiltration of the kMT cluster by non-kMTs, and near the pole the intermingling is even more pronounced (Fig. 8 *C*). This geometry would permit interactions between the two MT classes, so we have carried out a neighbor density analysis, as described in Materials and Methods, to see whether a morphometric approach might reveal preferred distances between these two MT classes.

From Fig. 1, *A–D* and previous work (McDonald et al., 1991) it is clear that a 2-D neighbor density analysis is sufficiently sensitive to detect a peak in the distribution of spacings between interdigitating antiparallel MTs in the zone of overlap during late anaphase and telophase in PtK_1 cells. MTs of opposite polarity are preferentially associated at a center–center spacing of ~40 nm (Fig. 1 *D*), while MTs of like polarity from the same region show little or no preferred spacing (Fig. 1 *C*). A similar analysis of the spacings between kMTs and non-kMTs in a metaphase chromosomal fiber, however, shows no preferred spacing at any point along the fiber. There is a detectable maximum in the distribution of kMTs around kMTs immediately next to the kinetochore

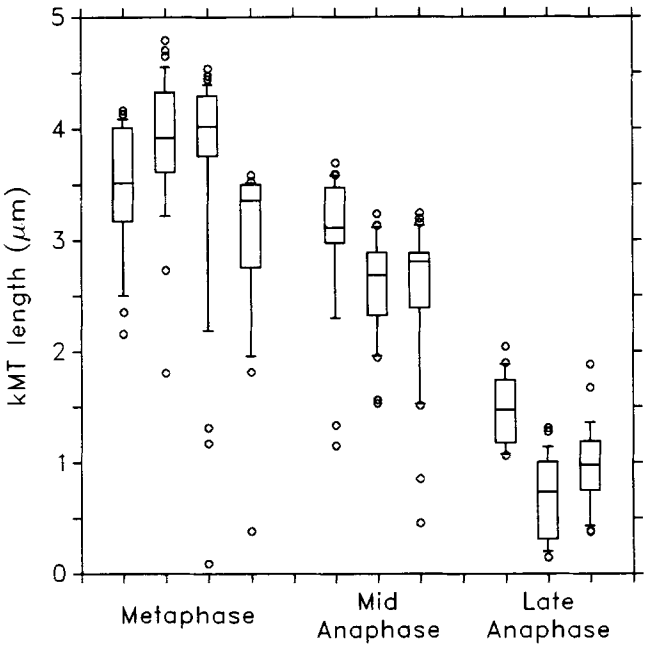

Figure 6. Tukey box plates of the lengths of kMTs at different stages of mitosis. Each column of data represents the kMTs from a single cell fixed at the stage of mitosis marked on the abscissa. The horizontal line within each rectangle indicates the median kMT length for that data set; the top and bottom of the rectangle are the 75th and 25th percentile, respectively; and the top and bottom horizontal marks show the 90th and 10th percentile. (○) Outlying data points.

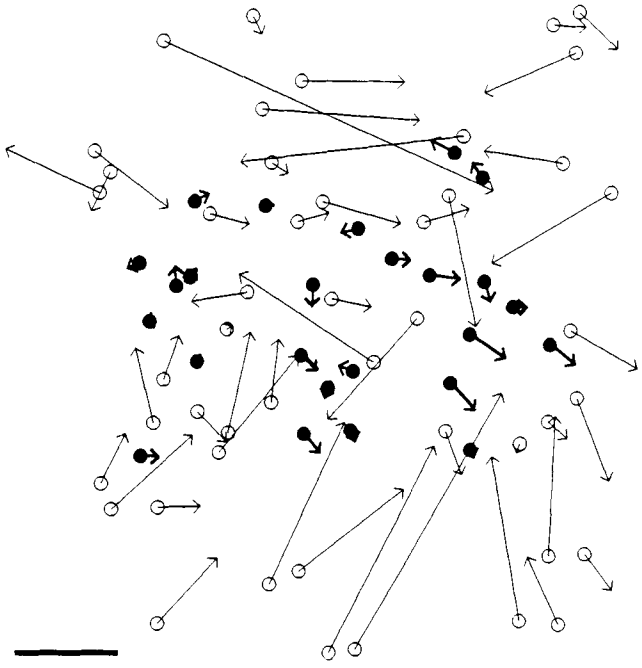

Figure 7. A vector display of the net cross-sectional movement of kMTs (●) and non-kMTs (○) from a metaphase chromosomal fiber, projected through nine sections. The kMTs tend to remain parallel to one another and show little change in position over this distance. Many of the non-kMTs have large changes in position, often passing into the kinetochore bundle and approaching individual kMTs at oblique angles. Tips of dark arrows mark the pole-proximal ends of kMTs; tips of light arrows mark the pole-proximal ends of non-kMTs. Bar, 200 nm.

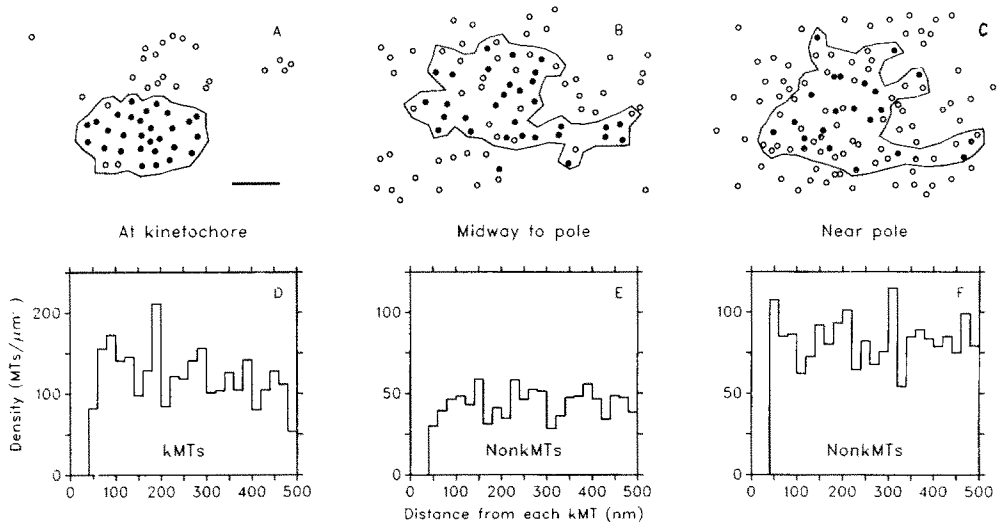

Figure 8. Cross sections through selected regions along the metaphase chromosomal fiber from the model shown in Fig. 4 *A*. (*A*) The region at the kinetochore; (*B*) a region from the middle of the bundle; and (*C*) a region at the pole. (•) kMTs; (○) non-kMTs. There is an obvious mixing of the two MT classes as one approaches the pole. (*D–E*) Neighbor density plots for the MTs within the contours drawn in *A–C*. Near the kinetochore (*D*) there is a slightly preferred spacing of ~90 nm among neighboring kMTs. At the mid region of the bundle (*E*) and near the pole (*F*), kMTs and non-kMTs show no preferred spacing. Bar, 250 nm.

(Fig. 8 *D*), as one might expect from the clustering that can be seen in Fig. 8 *A*. Even here, however, the neighbor density distribution is sufficiently erratic that no clear-cut regularity is evident. As one moves halfway to the pole (Fig. 8 *B*), the two classes of MTs become intermingled, but the distribution of non-kMTs around kMTs shows no obvious maximum (Fig. 8 *E*). Even close the pole, there is still essentially no evidence for a preferred spacing between kMTs and non-kMTs (Fig. 8 *F*).

A similar analysis has been conducted for all of the reconstructed fibers. By pooling the results from the fibers at each mitotic stage, we have obtained descriptions of neighbor density that show less variability than the curves shown in Fig. 8. Fig. 9 shows the pooled neighbor density distributions from mid-anaphase, the stage when one might expect the greatest likelihood of meaningful MT–MT interactions. Fig. 9 *A* is the average distribution of kMTs around kMTs immediately next to the kinetochores; as in metaphase, a weak peak in the distribution is seen at ~90 nm center to center. Fig. 9 *B* shows the average distribution of non-kMTs around kMTs halfway between the kinetochores and the poles; again there is no peak in the distribution. Indeed the flatness of the distribution is even more evident in this graph, which portrays data from four sections from each of three fibers, than in the graphs of Fig. 8, *E* and *F*, which show data from a single fiber. Similar analyses of four metaphase and three late anaphase cells show the same pattern, both midway between the kinetochores and the poles, and at the poles (data not shown). We conclude that by the criterion of neighbor density distributions, there is no preferential spacing between kMTs and non-kMTs at any time from metaphase through anaphase.

3-D Analyses of the Minimum Distances between MTs in Chromosomal Fibers

While the MTs in the chromosomal fiber do not display the ordered spacings characteristic of the telophase interzone, the physiological data on spindle force generation suggest that there is some sort of mechanical connection between kMTs and non-kMTs. One possibility is that this linkage is achieved in the pericentriolar material by connections that are too amorphous to show up in the analysis described above. Certainly the data on spindle MT polarity (for example, see Euteneuer and McIntosh, 1981) suggest that linkages of the kind found in the interzone should not be important in the chromosomal fibers, where essentially all the MTs are parallel. Another possibility, however, is that there are connections between kMTs and non-kMTs, but that the mean angle between the two MT classes is so large, due perhaps to other structural constraints on their trajectories, that the MTs of the chromosomal fiber can interact over only a small fraction of their lengths.

When lines are skew in space, they are widely separated over much of their lengths. We supposed, therefore, that the lack of a strong peak in the 2-D neighbor density distribution might be because of the low frequency with which kMTs and non-kMTs could come close to one another. The validity of this concern is shown in Fig. 10, a stereo drawing of some kMTs (dark lines) and some non-kMTs (light lines) traced

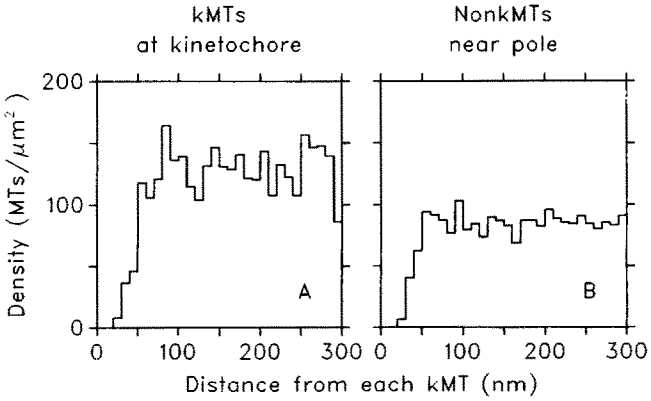

Figure 9. Average neighbor density plots from three data sets at mid anaphase. Near the kinetochores (*A*) there is a slight preference for a spacing of ~90 nm between kMT neighbors. Near the pole (*B*), kMTs and non-kMTs show no preferred spacing.

Figure 10. Stereo pair of a portion of a metaphase chromosomal fiber near the pole, where non-kMTs (*thin lines*) make many close approaches to kMTs (*thick lines*). All non-kMTs in this region that do not come close to kMTs have been eliminated from this display for clarity of viewing. The points of closest approach between kMT and non-kMT are indicated by a connecting line, but this is not meant to imply that there is a physical bridge between the two MTs. The appearance of two kMT bundles in this display results from the following facts: (*a*) that the region shown is from the place where the kMTs are most spread out; (*b*) that the magnification of the display is high; and (*c*) that the model has been rotated to an orientation which maximizes MT dispersal and hence image clarity.

through 15 sections near the polar region of a metaphase chromosomal fiber. The pole is on the right. The short vertical line segments mark all the positions where two MTs come to within 50 nm of one another. This particular volume was selected for display because it shows clearly the ways in which non-kMTs run past kMTs, approaching close only occasionally. If there were a preferred distance of closest approach between two kinds of MTs in 3-D, that preference would be greatly diluted in a 2-D neighbor density analysis by the greater inter-MT spacings that are so much more numerous. We therefore undertook to identify the 3-D distances of closest approach between each MT and all of its neighbors, as described in Materials and Methods, to see whether the resulting distances of closest approach might identify a regularity and/or specificity in the minimum inter-MT spacing.

The distributions of distances of closest approach show that MTs in the chromosomal fibers have a tendency to approach to within 30–50 nm, and that this tendency is most pronounced for the distances between kMTs and non-kMTs. Fig. 11, *A–C* show graphs of relative density versus distance obtained by averaging distributions from two chromosomal fiber reconstructions from the same cell in metaphase. The graphs all show a peak at 30–50 nm. This peak is strongest for the relative density of non-kMTs around kMTs (Fig. 11 *A*); the integral of the peak, after subtracting the average relative density at 100–200 nm, is 2.41, meaning that the average kMT has 2.41 non-kMTs approaching within 30–50 nm, in addition to those expected in a random distribution. The peaks are weaker in the distributions of densities of non-kMTs around each other (Fig. 11 *B*) or of kMTs around each other (Fig. 11 *C* and Table I).

Control data sets prepared by randomly shifting the positions of the MTs show that the peaks in the actual distributions involving non-kMTs cannot be explained simply by the packing of objects that do not approach more closely than a certain distance. To preserve the geometrical constraints inherent in the mixing of the two MT classes, we left the kMTs in their original positions and randomly shifted the non-kMTs by up to 60 nm. The probabilities of rejecting shifted positions that brought the MT too close to other MTs (see Materials and Methods) were adjusted so the rising phase of each graph of the relative density of non-kMTs around MTs of any type would match that of the actual graphs. This resulted in a good match for the rising phases of both graphs of particular interest (compare Fig. 11 *D* with *A* and 11 *E* with *B*). The averages of graphs from 20 separate randomizations (Fig. 11, *D* and *E*) do show peaks at ~40 nm, but the peaks are weaker than those seen in the real data and their falling phases are not as sharp as in the actual peaks. Further, the integrals of the peaks in the individual randomizations were never as large as those of the actual integrals (Table I). This is not because non-kMTs have been shifted out of the kinetochore bundles; note that the mean relative density in the control graphs at 100–200 nm is within 2% of the actual value. Thus, there appear to be preferred spacings between kMTs and non-kMTs that account for a substantial fraction of the tendency shown by these MTs to approach to within 30–50 nm.

We have also generated control graphs for the kMT to kMT distribution by randomly shifting the positions of each kMT up to 60 nm. The graph of the real data (Fig. 11 *C*) does not deviate significantly from the average of the controls (Fig. 11 *F*). Kinetochore MTs thus do not display the kind of specific inter-MT spacings characteristic of the relationship between kMTs and non-kMTs.

Similar results have been obtained from the analysis of our other reconstructions of metaphase and mid-anaphase chromosomal fibers. Each data set was examined separately, then actual and control integrals were computed by pooling the sets into 4 groups: the two metaphase sets just described; the two other metaphase sets, which were both from a different cell; the three mid-anaphase sets, which were all from the same cell; and two of the late anaphase sets that were from the same cell. The density graphs were all similar to those seen in Fig. 11, except that the other metaphase sets showed a pronounced peak in the kMT to kMT distribution. The actual and control integrals are listed in Table I. The actual in-

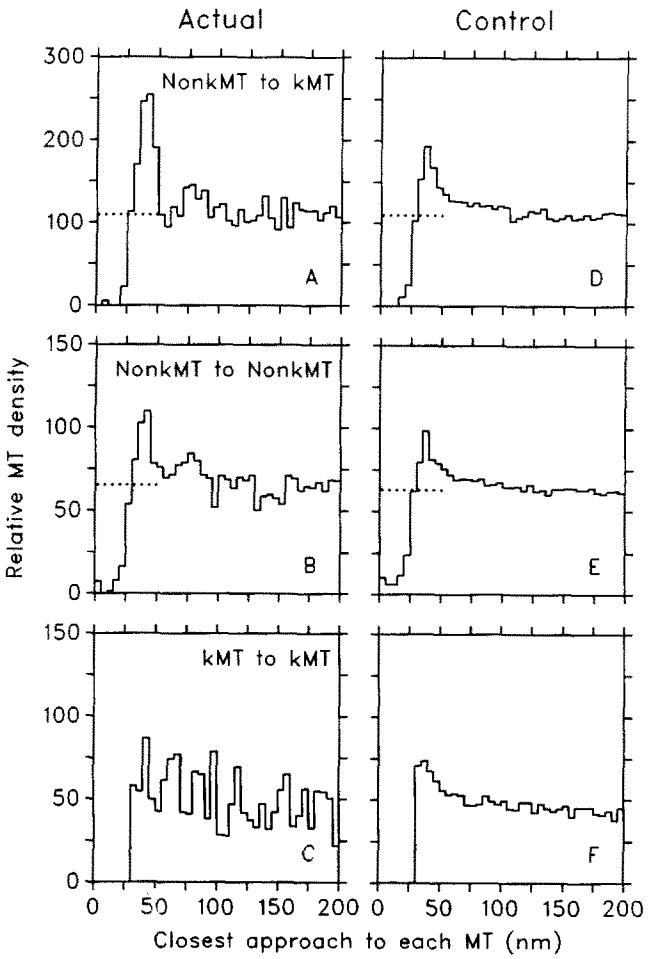

Figure 11. Distributions of distances of closest approach between MTs in 3-D. Distributions were scaled as described in Materials and Methods to obtain relative density values. The graphs show the sum of results from two chromosomal fibers from a single metaphase cell. (*A–C*) Based on actual MT positions; (*D–F*) the sum of results after randomly shifting MT positions 20 different times (non-kMTs shifted for *D* and *E*, kMTs shifted for *F*). (*A* and *D*) Distances from kMTs to non-kMTs. (*B* and *E*) Distances from non-kMTs to non-kMTs. (*C* and *F*) Distances from kMTs to kMTs.

tegrals for metaphase and mid-anaphase were all different from the control values. The strength of this spacing regularity appears to decline somewhat from metaphase to mid-anaphase and falls even more by late anaphase (Table I), but the physiological significance of this change is hard to assess.

Our ability to make the rising phase of control graphs match the comparable features of the real density data is a potentially important feature of these tests; it represents an advance over previous tests of the proposition that preferred distances between MTs arise simply from crowding (for example, see McDonald et al., 1979). When no effort is made to match the rising phases, and a range of close distances is simply forbidden, then the imposed constraint introduces a weak peak in the first non-zero bin of the density graph and a monotonic decay to the baseline level (Fig. 11 *F* approaches this behavior). Because the peaks in the real data have a different shape, the comparison between actual and control integrals is then quite sensitive to the choice of the bins used for integration. Matching the rising phase not only

Table I. Integrals of Peaks in Distributions of Nearest Distances between MTs

Stage	Distribution	Actual	Control
Metaphase	kMT to non-kMT	2.41	1.30 ± 0.21
(n = 2)	non-kMT to non-kMT	0.65	0.47 ± 0.08
Metaphase	kMT to non-kMT	2.13	0.93 ± 0.23
(n = 2)	non-kMT to non-kMT	1.11	0.65 ± 0.11
Mid-anaphase	kMT to non-kMT	2.08	1.31 ± 0.18
(n = 3)	non-kMT to non-kMT	0.82	0.53 ± 0.07
Late anaphase	kMT to non-kMT	0.49	
(n = 2)	non-kMT to non-kMT	0.06	

Two or three reconstructions were averaged for each set of values, as indicated. Integrals are the number of non-kMTs making close approaches to the typical kMT (for kMT to non-kMT) or to the typical non-kMT (for non-kMT to non-kMT), minus the number expected from the relative density at 100–200 nm. Each control value is based on 40 randomized sets. In each case, none of the 40 individual sets gave integrals as large as the actual value. The area within which the MTs were shifted was a 100-nm square for 20 sets and a circle of 120-nm diam for 20 sets.

provides a more realistic test, but also makes the control peak more similar in shape to the actual one and thus facilitates quantitative comparison by making the difference between actual and control integrals depend much less on boundaries used for integration.

We have identified two biases that should contribute in opposite directions to the values of the control integrals, but their effects are probably far too small to account for the differences seen between the actual and the control integrals. First, 4–8 MTs had to be shifted by more than 60 nm to avoid approaching other MTs too closely. However, even if all of those MTs were moved completely out of the region where they could pass near kMTs (which is itself unlikely), they would account for only 0.15–0.3 non-kMTs per kMT, much less than the difference between the actual and control integrals (0.7–1.2). On the other hand, 2–5 non-kMTs had to be left in their original positions, where they probably did approach kMTs closely. The control integrals were probably biased slightly upward by these MTs, reducing the differences that should have been seen between actual and control values. In sum, however, these effects are small, and the differences between actual and control integrals suggest that kMTs and non-kMTs frequently approach each other at a well-defined spacing.

Specific spacings between MTs could result from physical connections. In Fig. 10 the vertical bars mark positions of close approach; they are not representations of true cross bridges. To see whether the distances of closest approach were in fact accompanied by identifiable cross-bridges, models in which the regions of proximity were identified, e.g., the vertical lines in Fig. 10, were used as graphic overlays on successive spindle cross sections. We examined the electron micrographs for evidence of well defined bridges, but found that the spaces between the MTs were not distinguishable from background staining. If true bridges are responsible for the spacing preferences seen, either our fixation has not preserved them or our sections are not sufficiently thin for the bridges to be obvious.

Fig. 10 also shows that kMTs and non-kMTs are oriented at substantial angles to one another as they pass. For a typical data set, the angles between kMTs and non-kMTs at their points of closest approach had a mean ± SD of 33±17°. This

high value suggests that the two MT classes would have a considerable problem in forming strong bonds.

Discussion

This study presents a quantitative fine structural analysis of chromosomal fibers from the spindles of mammalian mitotic cells fixed with methods designed to optimize the preservation of cytoskeletal elements. Both the kMTs and the non-kMTs that accompany them have been traced, and spatial relationships between the two MT classes have been analyzed. We have learned that most kMTs run all the way from the kinetochore to the vicinity of the pole throughout metaphase and anaphase. Many non-kMTs invade this MT bundle, but there is no evidence from the neighbor density distributions for strong interactions between kMTs and non-kMTs. Apparently much of the strength of the mechanical linkage between kMTs and the rest of the spindle is achieved through the pericentriolar material. Nonetheless, a 3-D analysis of the minimum distances between neighboring MTs suggests that there is a weak interaction between kMTs and non-kMTs as the two run to the poles.

Practical Considerations

The chemical fixation procedure used here was developed using cultured mammalian cells to optimize the preservation of cytoplasmic MTs and microfilaments (McDonald, 1984). We think that it gives a reliable preservation of spindle fine structure, both because spindle MTs in the resulting preparations are numerous and follow smooth trajectories and because spindle vesicles are numerous, smooth, and most of them are circular.

The quality of our 3-D models is dependent on the reliability of our recognition of MTs in spindle cross sections. While we have used computational methods for pattern recognition to identify many of the MT images, the ultimate accuracy of our MT identifications is based on the ability of a trained biologist to make this determination. All our computer-generated models were checked by eye, using the 12 megabyte memory of our image display to store both electron micrographs of successive serial sections and images of the draft model. Rapid riffling through these carefully aligned images greatly increased an observer's ability to identify MTs and to follow them through the sections. Our automatic MT identification methods were highly effective for MTs that were approximately perpendicular to the section plane, but they often failed where the MTs were too oblique. In these cases, the operator checking the model had to add quite a few points to make the model accurate. It was encouraging to see, however, that once these corrections had been made by one operator, a second operator would change the model almost not at all.

kMT Length Distributions

Two previous studies of mammalian cells have looked at the structure of chromosomal spindle fibers (Rieder, 1981; Witt et al., 1981). In each case, these studies treated the cells before fixation by procedures that reduced the numbers of non-kMTs. Such treatments prohibited an analysis of the interaction between kMTs and non-kMTs, as presented here, and they may also have affected the structure of the kMTs themselves. Nonetheless, our distributions of kMT lengths in PtK cells are similar to those reported by Witt et al. (1981) for CHO cells, i.e., most of the kMTs extend from the kinetochore to the vicinity of the pole. Our results differ, however, from those of Rieder (1981), who reconstructed the chromosomal fiber of PtK cells after cold treatment. While he found about the same number of kMTs per chromosome, a larger number of his kMTs ended farther from the pole than in our study. His fibers also included a number of MTs that originated at the pole but did not extend all the way to the kinetochore; we found only a few such MTs. Finally, the MT packing within the fibers studied by Rieder (1981) was tighter than that which we have seen, presumably because of the cold treatment.

The chromosomal fibers in cold-treated crane fly spermatocytes described by Scarcello et al. (1986) are similar to the ones described by Rieder, though they contain more kMTs. Cells fixed at physiological temperatures, on the other hand, contained kMTs with a wide range of lengths, only a few of which were long enough to reach the spindle poles. The reasons for the differences between this arrangement and what we have described remain to be determined.

The chromosomal fiber structure described here is compatible with the view that most kMTs are derived from MTs initiated by the centrosomes through the capture of their plus ends at or near the kinetochores (Schrader, 1953; Tippit et al., 1980; Euteneuer and McIntosh, 1981; Kirschner and Mitchison, 1986; Hayden et al., 1990). The neighbor density of kMTs at all the kinetochores examined was rather uniform, but showed no sharp peak or lattice-like arrangement. We suppose that chromosomes define their kMTs by binding MTs to sites previously established by the structure of the kinetochore, but our data suggest that these sites are not well ordered in the plane of the kinetochore.

The poleward ends of most of the kMTs in our reconstructions are near the pericentriolar material, but none extend to the immediate vicinity of the centrioles. Indeed, many non-kMTs continue farther poleward than even the longest of the kMTs, and some of the kMTs end outside the pericentriolar material, as defined by the osmiophilic matrix. This observation raises the question of how best to define the volume that should be called the spindle pole. A sensible answer will depend on identifying the functionally significant components of the pericentriolar material and localizing them together with the minus ends of spindle MTs. Nonetheless, our observations are consistent with the idea that the kMTs are pulled away from the pole by forces generated at the kinetochore (Hyman and Mitchison, 1991). This tension should strain the material that tethers the kMTs to the pericentriolar material. Such a strain may bear the load that is required to keep each chromosome attached to the pole while spindle motors are pulling on its kinetochore and related factors are promoting kMT disassembly. Since non-kMTs penetrate farther into the pericentriolar material than kMTs, these MTs may be pushed toward the poles by forces generated where they interdigitate near the spindle midzone, as in diatoms (reviewed in Hogan and Cande, 1990).

The fact that the spread in the kMT length distribution is rather well preserved during anaphase is consistent with other observations that kMT shortening is accomplished largely by subunit loss at the kinetochores (Mitchison et al., 1986; Gorbsky and Borisy, 1988; Nicklas, 1989).

3-D Models of kMT Trajectories

The light microscope observations of Cassimeris et al. (1989) and the "zipping" model of anaphase chromosome movement proposed by Bajer (1973) both predict that the poleward ends of kMTs should flare out as a result of their interactions with non-kMTs. Our reconstructions of kMT trajectories show that this is not the case in PtK cells; the kMTs in anaphase cells remain more or less parallel throughout the length of the fiber bundle. This arrangement is again consistent with the view that the kMTs lose most of their subunits during anaphase at the kinetochore, and it suggests that the non-kMTs and/or the pericentriolar material provides a structure that is both sufficiently stable to withstand the mechanical stresses placed on the kMTs and sufficiently active to permit the slow flux of MTs toward the pole that is seen during metaphase (Mitchison, 1989; Sawin and Mitchison, 1990). The location of the kMT minus ends at some distance from the nearest centriole emphasizes the importance of the pericentriolar material in spindle mechanics and MT behavior.

Interactions between kMTs and non-kMTs

No published study of a metazoan spindle has previously assessed the neighbor density distributions of kMTs and non-kMTs. There is, however, some evidence from lower eukaryotes that these two MT types do not adopt any specific inter-MT spacing. Heath (1974) studied the fungus *Thraustotheca*, and found that the single kMT attached to each chromosome made a connection to the spindle pole body. However, it appeared to be spaced too far from other MTs to interact with them. Tippit et al. (1983) used a neighbor density analysis analogous to the one used here and elsewhere (McDonald et al., 1979) to look at possible kMT-non-kMT interactions in the alga *Ochromonas*, but they failed to find them. In this cell type there are only a few MTs per kinetochore, and since the data analysis was carried out by hand, it was not feasible to look at a large number of spacings to try to pick out a weak effect. The data presented here are collected from an organism in which there is an average of 25 MTs per kinetochore, and where non-kMTs mingle with kMTs over much of the distance between chromosome and pole. In addition, our methods have allowed us to examine over 1,000 pair-wise spacings for each stage of mitosis analyzed. Nonetheless, a 2-D neighbor density analysis yielded no evidence for a specific MT spacing of the kind detected in the mid-region of the anaphase interzone (McDonald et al., 1979; McIntosh et al., 1985; and compare Fig. 1 with Figs. 8 and 9).

Several mechanical experiments demonstrate that chromosomes are anchored to the spindle by linkages that can withstand considerable stress (reviewed in Nicklas, 1989). Certainly chromosome movement through a viscous medium should impose a load on the kMTs, and unless this load is borne by connecting the kMTs to something, the kMTs should move toward the metaphase plate, rather than the chromosomes moving toward the poles. Of additional interest is the study in which manipulated chromosomes were characterized in a living cell, then the same chromosomes and their fibers were analyzed by serial section EM by Nicklas et al. (1982). The light microscope observations showed that chromosome fibers were firmly anchored at the pole and that when the chromosomes were moved laterally across the spindle, there were few restrictions to fiber movement except in a region very near the pole. Serial section reconstructions of the MTs in this region showed that some non-kMTs became bent in such a way as to suggest an interaction between kMTs and non-kMTs. While our finding of no strong peak in the neighbor density analysis of kMTs versus non-kMTs is consistent with previous structural work on small spindles, it seems inconsistent with aspects of the physiology and mechanics of spindle action.

Through viewing serial sections displayed in rapid succession on the video monitor, we learned that kMTs and non-kMTs intermingle and might be interacting at single points of close approach. When the 3-D trajectories of the two MT types were compared, we found that there was, in fact, a rather consistent distance of closest approach as the skew curves passed each other. Our analysis of this phenomenon suggests that the closest distance seen occurs far more likely than one would expect by chance, consistent with a model that posits a weak interaction between kMTs and non-kMTs.

It is difficult to evaluate the physiological significance of this prevalent distance of closest approach. Inter-MT bridges have been described in spindles (for example, see Hepler et al., 1970) but examination of the places where the kMTs and non-kMTs came close showed only a few recognizable bridges of this type. We conclude that our morphometric method has uncovered an interaction that is likely to be mechanically weak. We infer that much of the mechanical structure which tethers the minus ends of kMTs near the pole is based on interactions between MTs and the pericentriolar material of the centrosome. This inference poses a problem in understanding the experiment by Nicklas, in which all the MTs between chromosome and pole were cut with a glass needle, yet the chromosomes continued to move up toward the edge of the cut (Nicklas, 1989). Either the apparently weak interactions described here are sufficient to support the load of chromosome motion or the act of truncating the spindle served to attach some spindle MTs to the glass substrate, providing a mechanically sufficient substitute for the normal spindle pole.

Our observations of an essentially continuous connection between kinetochore and pole in a metazoan, as well as the lack of evidence for strong interactions between kMTs and non-kMTs suggest that the coupling of MTs to the pericentriolar material is one of the real mechanical significance for spindle action. This suggestion is broadened by the recent indications that spindle MTs move toward the poles throughout prometaphase and anaphase (Mitchison, 1989; Sawin and Mitchison, 1991). While we have not yet identified any well-defined structures that might accomplish this mechanically significant connection, physiological evidence tells us that they exist. Future structural studies will be directed toward an effort to preserve and visualize these features of spindle morphology.

We thank W. Z. Cande (University of California, Berkeley, CA) in whose lab some of the early stages of this were begun for his hospitality and encouragement.

This study was supported largely by grants CD425 from the American Chemical Society and RR00592 from the National Institutes of Health to J. R. McIntosh.

Received for publication 27 December 1991 and in revised form 16 April 1992.

References

Aist, J. R. and C. J. Bayles. 1991. Ultrastructural basis of mitosis in the fungus *Nectria haematococca*. I. Asters. *Protoplasma.* 161:111–122.

Aist, J. R., and M. W. Berns. 1981. Mechanics of chromosome separation during mitosis in *Fusarium* (Fungi imperfecti): new evidence from ultrastructural and laser microbeam experiments. *J. Cell Biol.* 91:446–458.

Bajer, A. 1973. Interaction of microtubules and the mechanism of chromosome movement (Zipper hypothesis). *Cytobios.* 8:139–160.

Boots, B. N., and A. Getis. 1988. Point Pattern Analysis. Sage Publications, Newbury Park, CA. 93 pp.

Cassimeris, L., S. Inoue, and E. D. Salmon. 1988. Microtubule dynamics in the chromosomal spindle fiber: analysis by fluorescence and high-resolution polarization microscopy. *Cell Motil. Cytoskeleton.* 10:185–196.

Cleveland, W. S. 1985. The Elements of Graphing Data. Wadsworth Advanced Books and Software, Monterey, CA. 129–134.

Euteneuer, U., and J. R. McIntosh. 1981. Structural polarity of kinetochore microtubules in PtK1 cells. *J. Cell Biol.* 89:338–345.

Fuge, H. 1985. The 3-D architecture of chromosome fibers in the crane fly II. Amphitelic sex univalents in meiotic anaphase I. *Chromosoma (Berl.).* 91:322–328.

Gorbsky, G. J., P. J. Sammak, and G. G. Borisy. 1988. Microtubule dynamics and chromosome motion visualized in living anaphase cells. *J. Cell Biol.* 106:1185–1192.

Hamaguchi, M. S., and Y. Hiramoto. 1986. Analysis of the role of astral rays in pronuclear migration in sand dollar eggs by the colcemid-UV method. *Devel. Growth & Differ.* 28:143–156.

Hayden, J. H., S. S. Bowser, and C. L. Rieder. 1990. Kinetochores capture astral microtubules during chromosome attachment to the mitotic spindle: direct visualization in live newt lung cells. *J. Cell Biol.* 111:1039–1045.

Heath, I. B. 1974. Mitosis in the fungus *Thraustotheca clavata*. *J. Cell Biol.* 60:204–220.

Heath, I. B. 1980. Variant mitoses in lower eukaryotes: indicators of the evolution of mitosis? *Int. Rev. Cytol.* 64:1–80.

Hepler, P. K., J. R. McIntosh, and S. Cleland. 1970. Intermicrotubule bridges in the mitotic spindle apparatus. *J. Cell Biol.* 45:438–445.

Hogan, C. J., and W. Z. Cande. 1990. Antiparallel microtubule interactions: spindle formation and anaphase B. *Cell Motil. Cytoskeleton.* 16:99–103.

Hyman, A. A. 1989. Centrosome movement in the early divisions of *Caenorhabditis elegans*: a cortical site determining centrosome position. *J. Cell Biol.* 109:1185–1193.

Hyman, A. A., and T. J. Mitchison. 1991. Two different microtubule based motor activities with opposite polarities in kinetochores. *Nature (Lond.).* 351:206–211.

Jensen, C. G. 1982. Dynamics of spindle microtubule organization: kinetochore fiber microtubules of plant endosperm. *J. Cell Biol.* 92:540–558.

Kirschner, M., and T. Mitchison. 1986. Beyond self-assembly: from microtubules to morphogenesis. *Cell.* 45:329–342.

Leslie, R. J., and J. D. Pickett-Heaps. 1983. Ultraviolet microbeam irradiations of mitotic diatoms. Investigation of spindle elongation. *J. Cell Biol.* 96:548–561.

Masuda H., K. L. McDonald, and W. Z. Cande. 1988. The mechanism of anaphase spindle elongation: uncoupling of tubulin incorporation and microtubule sliding during in vitro spindle reactivation. *J. Cell Biol.* 107:623–633.

McDonald, K. L. 1984. Osmium-ferricyanide fixation improves microfilament preservation and membrane visualization in a variety of animal cell types. *J. Ultrastruct. Res.* 86:107–118.

McDonald, K. L. 1989. Mitotic spindle, ultrastructure and design. *In* Mitosis: Molecules and Mechanisms. J. S. Hyams and B. R. Brinkley, editors. Academic Press, Inc. New York. 1–38.

McDonald, K. L., M. K. Edwards, and J. R. McIntosh. 1979. The cross-sectional structure of the central mitotic spindle of *Diatoma vulgare*: evidence for specific interactions between antiparallel microtubules. *J. Cell Biol.* 83:443–460.

McDonald, K. L., J. D. Pickett-Heaps, J. R. McIntosh, and D. H. Tippit. 1977. On the mechanism of anaphase spindle elongation in *Diatoma vulgare*. *J. Cell Biol.* 74:377–388.

McDonald, K., D. Mastronarde, E. O'Toole, R. Ding, and J. R. McIntosh. 1991. Computer-based tools for morphometric analysis of mitotic spindles and other microtubule systems. *EMSA Bull.* 21:47–53.

McIntosh, J. R., and G. E. Hering. 1991. Spindle fiber action and chromosome movement. *Annu. Rev. Cell Biol.* 7:403–426.

McIntosh, J. R., and S. C. Landis. 1971. The distribution of spindle microtubules during mitosis in cultured human cells. *J. Cell Biol.* 49:468–497.

Mitchison, T. J. 1988. Microtubule dynamics and kinetochore function in mitosis. *Annu. Rev. Cell Biol.* 4:527–550.

Mitchison, T. J. 1989. Polewards microtubule flux in the mitotic spindle: evidence from photoactivation of fluorescence. *J. Cell Biol.* 109:637–652.

Mitchison, T. J., and M. W. Kirschner. 1985. Properties of the kinetochore in vitro. II. Microtubule capture and ATP-dependent translocation. *J. Cell Biol.* 101:766–776.

Mitchison, T. J., L. Evans, E. Schulze, and M. Kirschner. 1986. Sites of microtubule assembly and disassembly in the mitotic spindle. *Cell.* 45:515–527.

Moore, M. J. 1975. Removal of glass coverslips from cultures flat embedded in epoxy resins using hydrofluoric acid. *J. Microsc. (Oxf.).* 104:205–207.

Nicklas, R. B. 1988. The forces that move chromosomes in mitosis. *Annu. Rev. Biophys. Biophys. Chem.* 17:431–449.

Nicklas, R. B. 1989. The motor for poleward chromosome movement in anaphase is in or near the kinetochore. *J. Cell Biol.* 109:2245–2255.

Nicklas, R. B., and D. F. Kubai. 1985. Microtubules, chromosome movement, and reorientation after chromosomes are detached from the spindle by micromanipulation. *Chromosoma (Berl.).* 92:313–324.

Nicklas, R. B., D. F. Kubai, and T. S. Hays. 1982. Spindle microtubules and their mechanical associations after micromanipulation in anaphase. *J. Cell Biol.* 95:91–104.

Paweletz, N. 1967. Zur Funktion des "Fleming-Korpers" bei der Teilung tierscher Zellen. *Naturwissenschaften.* 54:533–535.

Rieder, C. L. 1981. The structure of the cold-stable kinetochore fiber in metaphase PtK cells. *Chromosoma (Berl.).* 84:145–148.

Rieder, C. L. 1982. The formation, structure and composition of the mammalian kinetochore and kinetochore fiber. *Int. Rev. Cytol.* 79:1–58.

Rieder, C. L. 1990. Formation of the astral mitotic spindle: ultrastructural basis for the centrosome-kinetochore interaction. *Electron Microsc. Rev.* 3:269–300.

Rodieck, R. W. 1991. The density recovery profile: a method for the analysis of points in the plane applicable to retinal studies. *Visual Neurosci.* 6:95–111.

Sawin, K. E., and T. J. Mitchison. 1991. Poleward microtubule flux in mitotic spindles assembled in vitro. *J. Cell Biol.* 112:941–954.

Sawin, K. E., and J. M. Scholey. 1991. Motor proteins in cell division. *Trends Cell Biol.* Vol. 1, 122–129.

Saxton, W. M., and J. R. McIntosh. 1987. Interzone microtubule behavior in late anaphase and telophase spindles. *J. Cell Biol.* 105:875–886.

Scarcello, L. A., M. A. Janicke, and J. R. LaFountain, Jr. 1986. Kinetochore microtubules in crane fly spermatocytes: untreated, 2°-treated, and 6°-grown spindles. *Cell Motil. Cytoskeleton.* 6:428–438.

Schibler, M. J., and J. D. Pickett-Heaps. 1987. The kinetochore fiber structure in the acentric spindles of the green alga *Oedogonium*. *Protoplasma.* 137: 29–44.

Schrader, F. 1953. Mitosis. Columbia University Press, New York. 1–170.

Tippit, D. H., K. L. McDonald, and J. D. Pickett-Heaps. 1975. Cell division in the centric diatom *Melosira varians*. *Cytobiologie.* 12:52–73.

Tippit, D. H., J. D. Pickett-Heaps, and R. Leslie. 1980. Cell division in two large pennate diatoms *Hantzschia* and *Nitzschia*. III. A new proposal for kinetochore function during prometaphase. *J. Cell Biol.* 86:402–416.

Tippit, D. H., L. Pillus, and J. D. Pickett-Heaps. 1983. Near neighbor analysis of spindle MTs in the alga *Ochromonas*. *Eur. J. Cell Biol.* 30:9–17.

Vorobjev, I. A., and E. S. Nadezhdina. 1987. The centrosome and its role in the organization of microtubules. *Int. Rev. Cytol.* 106:227–293.

Witt, P. L., H. Ris, and G. G. Borisy. 1981. Structure of kinetochore fibers: microtubule continuity and inter-microtubule bridges. *Chromosoma (Berl.).* 83:523–540.